

Efficient Decoding Algorithms for Polar Codes based on 2×2 Non-Binary Kernels

Peihong Yuan, Fabian Steiner
Institute for Communications Engineering
Technical University of Munich
Munich, Germany
{peihong.yuan,fabian.steiner}@tum.de

Abstract—Polar codes based on 2×2 non-binary kernels are discussed in this work. The kernel over $\text{GF}(q)$ is selected by maximizing the polarization effect and using Monte-Carlo simulation. Belief propagation (BP) and successive cancellation (SC) based decoding algorithms are extended to non-binary codes. Additionally, a successive cancellation list (SCL) decoding with a pruned tree is proposed. Simulation results show that the proposed decoder performs very close to a conventional SCL decoder with significantly lower complexity.

Index Terms—non-binary polar codes, kernel selection, decoding algorithm

I. INTRODUCTION

Polar codes were proposed in [1], [2] and they achieve the capacity of binary-input discrete memoryless channels asymptotically in the block length [1]. Due to their low complexity and excellent performance, polar codes have been adopted for the control channel in 5G enhanced mobile broadband (eMBB) [3].

Successive cancellation (SC) was the first decoding algorithm for polar codes but has poor performance at short or moderate block length. Successive cancellation list (SCL) decoding [4] improves the finite length performance significantly at the cost of higher latency, power and storage consumption. Another approach to improve decoding is successive cancellation flip (SCF) decoding [5]. SCF decoders try to identify and correct the first erroneous estimation during SC decoding by sequentially flipping the unreliable decisions. Belief propagation (BP) decoding algorithm for polar codes based on [6] was proposed in [7]. In contrast to the SC-based approaches, BP decoding provides the soft-output reliability information.

Low-density parity-check (LDPC) codes over non-binary Galois fields (GFs) were introduced in [8] and outperform binary LDPC codes at the cost of higher decoding complexity. Non-binary polar codes and their decoding algorithms were discussed in [9]–[12]. One advantage of non-binary codes is a natural fit to higher-order modulation: no symbol mapping and demapping operations are needed for q -ary modulation with codes over $\text{GF}(q)$.

In this work, we discuss non-binary polar codes based on the non-binary extension of the Arıkan kernel. The kernel is selected by Monte-Carlo simulation to maximize the polarization effect. The SC-based and BP decoding algorithms are extended

to non-binary symbols by using the message passing rule in the probability-domain proposed in [8]. The fast Fourier transform (FFT) based check node (CN) operation [13] reduces the CN complexity from $\mathcal{O}(q^2)$ to $\mathcal{O}(q \log_2 q)$. Additionally, a SCL algorithm with a pruned tree is proposed. Simulation results show that the proposed decoder performs very close to the conventional SCL decoder with significantly lower average computational complexity.

This work is organized as follows. In Sec. II, SC decoding over $\text{GF}(q)$ and the Monte-Carlo based kernel selection are introduced. In Sec. III, we extend BP, SCF and SCL decoding to the non-binary case and discuss the simulation results. SCL with a pruned tree is proposed in Sec. III-C. We conclude in Sec. IV.

II. POLAR CODING OVER $\text{GF}(q)$

A. Notations

Uppercase letters denote random variables (RVs) while the corresponding lowercase letters are their realizations. The notation c^n denote a vector of length n . P_X denotes the probability mass function (PMF) of a discrete RV X . We consider only GFs of order $q = 2^r$, $r > 1$. Binary and decimal representations are used to describe elements over GFs, i.e., $\text{GF}(q)$ has q elements and the elements can be represented by binary r -tuples or integers between 0 and $q - 1$.

For the codes over $\text{GF}(q)$, n_c denotes the code length in symbols, $n_{c,\text{bin}} = n_c r$ denotes the code length in bits, $k_{c,\text{bin}}$ is the code dimension in bits.

B. System Model

A non-binary polar code over $\text{GF}(q)$ of length n_c and dimension $k_{c,\text{bin}}$ is defined by the q -ary polar transform $\mathbb{F}^{\otimes \log_2 n_c}$ and $n_{c,\text{bin}} - k_{c,\text{bin}}$ frozen (bit) positions, where \mathbb{F} denotes the extended Arıkan kernel

$$\mathbb{F} = \begin{bmatrix} 1 & 0 \\ \alpha & \beta \end{bmatrix}, \quad \alpha, \beta \in \text{GF}(q) \quad (1)$$

and $(\cdot)^{\otimes}$ denotes the Kronecker power. Fig. 1 shows the basic q -ary polar transform of size $n_c = 2$. Polar encoding can be represented by

$$c^{n_c} = u^{n_c} \mathbb{F}^{\otimes \log_2 n_c}. \quad (2)$$

The vectors u^{n_c} , c^{n_c} and all (addition, multiplication) operations are defined over $\text{GF}(q)$. The vector c^{n_c} denotes the code

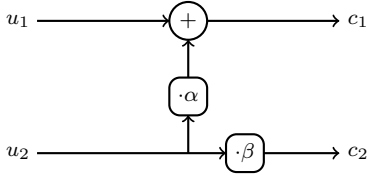


Figure 1: A 2×2 kernel over $\text{GF}(q)$, $\alpha, \beta \in \text{GF}(q)$.

symbols. The vector u^{n_c} can be represented by $n_{c,\text{bin}}$ bits and includes information bits and frozen bits. For a symbol $u_i \in \text{GF}(q)$, the first t_i bits can be selected as frozen, where $t_i = 0, \dots, r$. The choice of symbol u_i is then restricted to $0, \dots, 2^{r-t_i} - 1$ and the symbol carries $r - t_i$ bits of information (assuming that the left bit is most significant for the bit-to-symbol conversion). We define the set for all possibilities of symbol u_i as

$$\mathcal{S}(u_i) = \{0, \dots, 2^{r-t_i} - 1\}. \quad (3)$$

If $t_i = 0$, then $|\mathcal{S}(u_i)| = q$. If $t_i = r$, then $\mathcal{S}(u_i) = \{0\}$. We have

$$\sum_{i=1}^{n_c} \log_2 |\mathcal{S}(u_i)| = k_{c,\text{bin}}. \quad (4)$$

The code rate is given by $\frac{k_{c,\text{bin}}}{n_{c,\text{bin}}}$.

The transmission system with q -ary polar codes is shown in Fig. 2. The vector $u_b^{n_{c,\text{bin}}}$ includes k information bits m^k , ℓ_{CRC} cyclic redundancy check (CRC) bits and $n_{c,\text{bin}} - k - \ell_{\text{CRC}}$ frozen bits (preset to zero). We have $k_{c,\text{bin}} = k + \ell_{\text{CRC}}$ in this case. $u_b^{n_{c,\text{bin}}}$ is then converted into the symbol vector u^{n_c} . For a 2^w -input channel, the code symbol c_i is mapped into r/w channel symbols, where $r \geq w$ and w is a factor of r :

$$c_i \mapsto x_{i,1}, \dots, x_{i,r/w} = x_i^{r/w}, \quad i = 1, \dots, n_c \quad (5)$$

$$c^{n_c} \mapsto \left(x^{r/w}\right)^{n_c} = x^n \quad (6)$$

where $n = \frac{n_c r}{w} = \frac{n_{c,\text{bin}}}{w}$ denotes the number of channel uses.

The discrete time memoryless additive white Gaussian noise (AWGN) channel with a 2^w -amplitude shift keying (ASK) constellation is described by

$$Y_j = X_j + \sigma Z_j, \quad j = 1, \dots, n \quad (7)$$

where $X \in \mathcal{X} = \{\pm\Delta, \pm 3\Delta, \dots, \pm(2^w - 1)\Delta\}$ and Z^n is a string of n independent and identically distributed zero mean Gaussian RVs with variance one. The signal-to-noise ratio E_s/N_0 is given by $\frac{\mathbb{E}(X^2)}{\sigma^2}$, where $\mathbb{E}(\cdot)$ denotes expectation. At the receiver, the demapper computes the a posteriori probabilities (APPs) of X via

$$P_{X|Y}(x_j|y_j) = P_X(x_j) \frac{p_{Y|X}(y_j|x_j)}{\sum_{a \in \mathcal{X}} P_X(a) p_{Y|X}(y_j|a)} \quad (8)$$

where

$$p_{Y|X}(y_j|x_j) = \frac{1}{\sqrt{2\pi\sigma^2}} \exp\left(-\frac{(y_j - x_j)^2}{2\sigma^2}\right). \quad (9)$$

Let $P_{C|Y^{r/w},i}$ denote the PMF of code symbol C_i given the relevant channel outputs:

$$P_{C|Y^{r/w},i} = \left[P_{C_i|Y_i^{r/w}}(0|y_i^{r/w}), \dots, P_{C_i|Y_i^{r/w}}(q-1|y_i^{r/w}) \right] \quad (10)$$

where

$$P_{C_i|Y_i^{r/w}}(c_i|y_i^{r/w}) = \prod_{v=1}^{r/w} P_{X_{i,v}|Y_{i,v}}(x_{i,v}|y_{i,v}). \quad (11)$$

The PMFs of n_c code symbols $P_{C|Y^{r/w}}^{n_c}$ are delivered to the decoder. The decoder outputs the estimated information bits \hat{m}^k with the help of the CRC. The transmission rate of this system is $\frac{k}{n}$.

C. Message Passing on Non-Binary Graphs

Considering the decoder in the probability domain, each message is a PMF with q probabilities, i.e.,

$$P_A = [P_A(0), P_A(1), \dots, P_A(q-1)]. \quad (12)$$

We have three basic probability domain operations:

- Multiplication and addition:

We have $B = A\alpha$ and

$$P_A(\mu) = P_B(\mu\alpha), \quad \mu \in \text{GF}(q). \quad (13)$$

We can find a $q \times q$ permutation matrix $\Pi_{\cdot\alpha}$ such that

$$P_B = P_A \Pi_{\cdot\alpha} \quad (14)$$

$$P_A = P_B \Pi_{\cdot\alpha}^{-1}. \quad (15)$$

We can also find a permutation matrix $\Pi_{+\alpha}$ for addition

$$P_{A+\alpha} = P_A \Pi_{+\alpha}. \quad (16)$$

Note that $\Pi_{\cdot\alpha}$ and $\Pi_{+\alpha}$ depend on the primitive polynomial.

- Check node (CN) update:

The CN node computes the PMF P_{A+B} from P_A and P_B .

$$P_{A+B}(\mu) = \sum_{\substack{\mu_1, \mu_2 \in \text{GF}(q) \\ \mu_1 + \mu_2 = \mu}} P_A(\mu_1) P_B(\mu_2), \quad \mu \in \text{GF}(q). \quad (17)$$

We have

$$P_{A+B} = P_A \circledast P_B \quad (18)$$

where \circledast denotes the cyclic discrete convolution and the complexity is given by $\mathcal{O}(q^2)$ [8]. By applying the fast Hadamard transform (FHT), the discrete convolution is translated to element-wise multiplication, which reduces the complexity of the CN update to $\mathcal{O}(q \log_2 q)$. We have

$$P_{A+B} = \mathcal{H}(\mathcal{H}(P_A) \odot \mathcal{H}(P_B)) \quad (19)$$

where $\mathcal{H}(\cdot)$ denotes the FHT operation and \odot denotes the element-wise multiplication. Note that the FHT is self inverse, i.e., $\mathcal{H}(\cdot) = \mathcal{H}^{-1}(\cdot)$.

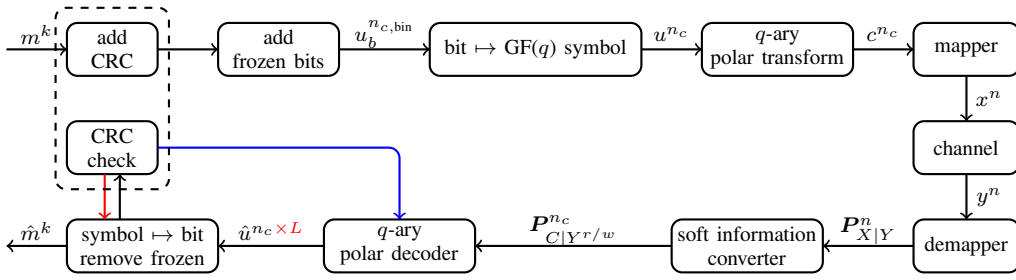


Figure 2: The 2^w -ASK transmission system with q -ary polar codes. The red part is only for SCL decoding and the blue part only for SCF decoding. $P_{X|Y}$ and $P_{C|Y^r/w}$ are PMFs and consist of vectors of w and q probabilities. In this work, the code symbols are not mapped into higher-order channel symbols, i.e., we have $w \leq r$.

- Variable node (VN) update:
The VN node computes the PMF of A from two different observed PMFs $P_{A,1}$ and $P_{A,2}$. We have

$$P_A(\mu) = P_{A,1}(\mu)P_{A,2}(\mu), \mu \in \text{GF}(q) \quad (20)$$

and

$$P_A = P_{A,1} \odot P_{A,2}. \quad (21)$$

The elements in the output message from the CNs and VNs must be normalized.

D. SC Decoding

The q -ary SC decoder follows mainly the implementation in [4, Algorithm 2-4]. Fig. 3 shows the extended recursive message update rules. We have

$$\begin{aligned} P'_1 &= a_1 \mathcal{H}(\mathcal{H}(P_1) \odot \mathcal{H}(P_2 \Pi_{\beta}^{-1} \Pi_{\alpha})) \\ &= a_1 \mathcal{H}(\mathcal{H}(P_1) \odot \mathcal{H}(P_2 \Pi_{\frac{\alpha}{\beta}})) \end{aligned} \quad (22)$$

$$P'_2 = a_2 \left(P_1 \Pi_{+\hat{u}_1} \Pi_{\alpha}^{-1} \right) \odot \left(P_2 \Pi_{\beta}^{-1} \right) \quad (23)$$

where the scalar a_1 and a_2 are the normalization factors that ensure that the probabilities in P'_1 and P'_2 sum up to 1. At the decoding phase i ($1 \leq i \leq n_c$), we get a conditional PMF of U_i by recursively updating the messages

$$P_{U_i|Y^{U^{i-1}}} = [\dots, P_{U_i|Y^{U^{i-1}}}(\mu|\mathbf{y}\hat{u}^{i-1}), \dots], \mu \in \text{GF}(q) \quad (24)$$

where \mathbf{y} denotes the channel output y^n . The hard decision of u_i is given by

$$\hat{u}_i = \underset{\mu \in \mathcal{S}(u_i)}{\text{argmax}} P_{U_i|Y^{U^{i-1}}}(\mu|\mathbf{y}\hat{u}^{i-1}). \quad (25)$$

E. Kernel Selection

From (22) and (23), we observe that the $P'_1(u_1)$ and $P'_2(u_2)$ depend only on the ratio $\frac{\alpha}{\beta}$. We now use a Monte-Carlo approach to choose the best ratio $\frac{\alpha}{\beta}$:

1. Set $u_1 = 0$ and select $u_2 \in \text{GF}(q)$ randomly.
2. q -ary encoding ($n_c = 2$): $c_1 = u_1 + u_2\alpha$ and $c_2 = u_2\beta$.
3. Map c_1 and c_2 to the 2^w -ary channel symbols ($w \leq r, n = \frac{2r}{w}$).
4. Add noise σZ^n and compute $P'_2(u_2)$.

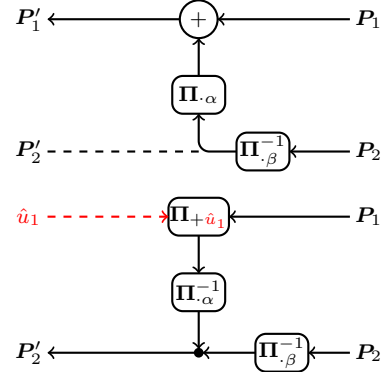


Figure 3: Message update rules for q -ary SC decoder.

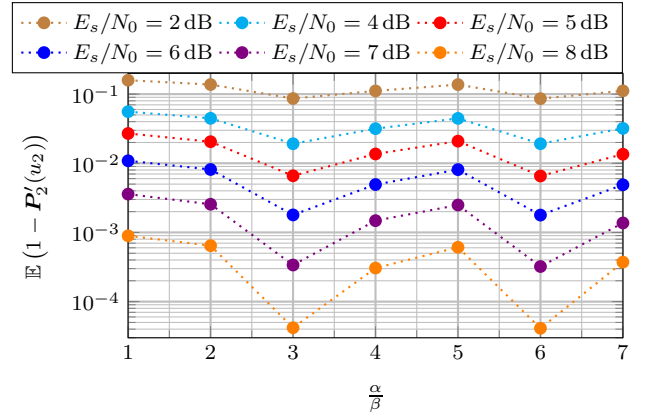


Figure 4: Reliability of “single-level” polarization over $\text{GF}(8)$, primitive polynomial = 11, $w = 1$

Note that $P'_2(u_2)$ is now a RV depending on σZ^n . Monte-Carlo simulation is used to find the optimal $\frac{\alpha}{\beta}$ which maximizes the “single-level” polarization effect, i.e., we choose

$$\frac{\alpha}{\beta} = \underset{\frac{\alpha}{\beta} \in \text{GF}(q)}{\text{argmin}} \mathbb{E}(1 - P'_2(u_2)). \quad (26)$$

An example for $\text{GF}(8)$ with binary input AWGN (biAWGN) is shown in Fig. 4. We observe that the ratios $\frac{\alpha}{\beta} = 3$ and $\frac{\alpha}{\beta} = 6$ provide the strongest “single-level” polarization for any channel qualities. We summarize good kernels for GFs for other field orders in Table I.

Table I: Good kernels for $\text{GF}(q)$, $q = \{4, 8, 16, 32, 64, 128, 256\}$, $w = 1$

q	Primitive Polynomial	$\frac{\alpha}{\beta}$
4	7	2, 3
8	11	3, 6
16	19	6, 7
32	37	13, 15, 21, 26
64	67	38, 50
128	137	57, 105
256	285	23, 29, 102, 131, 133, 81, 145, 212

III. IMPROVED DECODERS FOR NON-BINARY POLAR CODES

A. BP Decoding

BP decoding of non-binary polar codes is a message passing algorithm on the encoding graph. We use the flooding schedule in [14, Sec. II-B] with the q -ary message passing rules described in Sec. II-C. The early stopping criteria [15] is used, i.e., after every iteration, we check whether $\hat{c}^{n_c} = \hat{u}^{n_c} \mathbb{F}^{\otimes \log_2 n_c}$. If this is the case, the estimate \hat{u}^{n_c} is accepted. The decoder stops further iterations and outputs \hat{u}^{n_c} . The decoding complexity is upper bounded by the maximum number of BP iterations I_{\max} .

The block error rate (BLER) and average number of iterations (I_{avg}) of BP decoding with $I_{\max} = 20$ and 100 is shown in Fig. 5. We observe that the BP decoding ($I_{\max} = 100$) outperforms SC decoding by 0.4 dB with low average complexity/latency ($I_{\text{avg}} \leq 5$) in the high SNR regime (≥ 1.75 dB).

As a reference, we also provide simulation results for ultra sparse non-binary LDPC codes (with regular variable and check node degrees of two and four, respectively) [16] over $\text{GF}(256)$ with the same parameters and where the non-zero entries of the parity-check matrix have been chosen randomly from $\text{GF}(256)$. We observe that the non-binary LDPC code outperforms the polar code by 0.5 dB with BP decoding ($I_{\max} = 100$). Further improvements for polar BP decoding proposed in [17], [18] can be extended to the non-binary case.

B. SCF Decoding

Due to the serial nature of SC decoding, an erroneous bit decision can be caused by the channel noise or previous erroneous bit estimates. The main idea of SCF decoding [5] is trying to correct the first erroneous bit decision by sequentially flipping the unreliable decisions. The authors in [5] use an oracle-assisted SC decoder (SCO-1) to describe the potential benefits of correcting the first error. SCO-1 is a SC decoder that can identify and correct the first bit error. In the non-binary case, SCF decoder tries to correct the first erroneous decision for the q -ary symbols. Fig. 6 shows the histogram of the number of errors caused by the channel noise. We observe that 98.1% of the block errors at 2.25 dB are corrected by SCO-1 decoder.

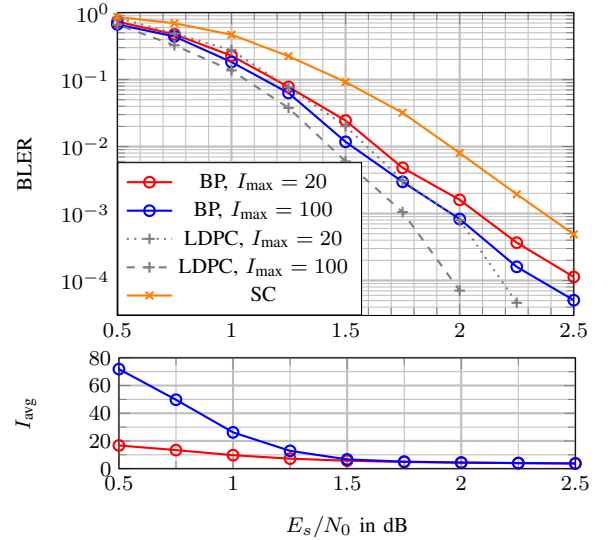


Figure 5: BP decoding performance of polar codes over $\text{GF}(256)$ on a bi-AWGN channel ($w = 1$), $n_c = 128$, $k = 512$, primitive polynomial = 285, $\alpha = 29$, $\beta = 1$, frozen position designed by Monte-Carlo method for SC decoding at 2.5 dB

Consider q -ary polar codes with rate $\frac{k+\ell_{\text{CRC}}}{n_c r} = \frac{k+\ell_{\text{CRC}}}{n_c \cdot \text{bin}}$. We use a ℓ_{CRC} bits CRC outer code to check whether the output is a valid codeword or not. The SCF decoder starts by performing SC decoding to generate the first estimation \hat{u}^{n_c} and stores the soft information in an $n_c \times (q-1)$ matrix \mathbf{A} :

$$\mathbf{A}_{i,\mu} = \begin{cases} \frac{P_{U_i|Y^{U^{i-1}}}(\mu|\mathbf{y}\hat{u}^{i-1})}{P_{U_i|Y^{U^{i-1}}}(\hat{u}_i|\mathbf{y}\hat{u}^{i-1})}, & \text{if } \mu \in \mathcal{S}(u_i) \\ 0, & \text{if } \mu \notin \mathcal{S}(u_i) \end{cases} \quad i = 1, \dots, n_c, \mu \in \text{GF}(q) \setminus \hat{u}_i. \quad (27)$$

If \hat{u}^{n_c} passes the CRC, the decoding is finished. In case the CRC fails, the SCF algorithm is given maximum T_{\max} attempts to correct the first symbol error. At the T -th attempt ($1 \leq T \leq T_{\max}$), the decoder finds the T -th largest element in \mathbf{A} . In case $\mathbf{A}_{i,\mu}$ is found, the SCF algorithm restarts the SC decoder by changing its estimate \hat{u}_i to μ . The CRC is checked after each attempt. This decoding process continues until the CRC passes or T_{\max} is reached. Note that the SCO-1 performance is a lower bound for SCF decoding.

The performance and decoding complexity of SCF on a bi-AWGN channel is shown in Fig. 7. A 16 bit CRC with generator polynomial $g_{\text{CRC}}(x) = x^{16} + x^{12} + x^5 + 1$ is used for error detection. We use the average number of attempts (T_{avg}) to describe the average complexity and latency of SCF decoding. We observe that SCF with $T_{\max} = 50$ performs very close to the SCO-1 bound. The average complexity and latency ($T_{\text{avg}} + 1$) converge to SC in the high SNR regime (≥ 1.75 dB), i.e., $T_{\text{avg}} + 1 \approx 1$.

C. SCL Decoding and SCL with Pruned Tree

SCL decoding was proposed in [4] and improves the performance of SC decoding by deploying L parallel SC decoding

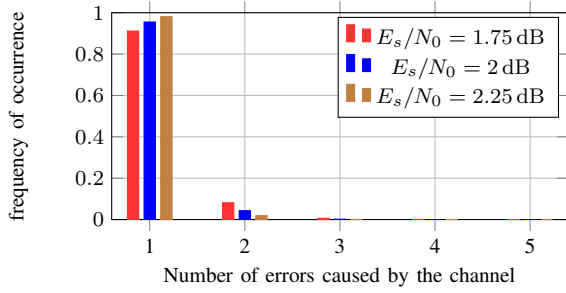


Figure 6: Frequency of the number of errors caused by the channel for polar codes over GF(256) on a biAWGN channel ($w = 1$), $n_c = 128$, $k = 512$, primitive polynomial = 285, $\alpha = 29$, $\beta = 1$, frozen position designed by Monte-Carlo method for SC decoding at 2.5 dB

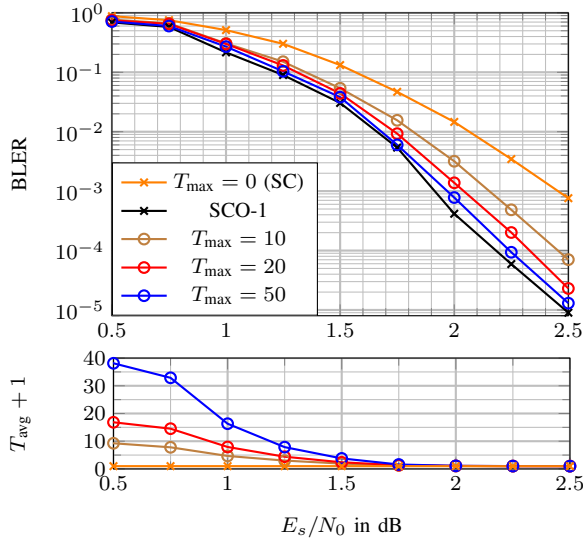


Figure 7: SCF decoding performance of polar codes over GF(256) on a biAWGN channel ($w = 1$), $n_c = 128$, $k = 512$, $\ell_{\text{CRC}} = 16$, primitive polynomial = 285, $\alpha = 29$, $\beta = 1$, frozen position designed by Monte-Carlo method for SC decoding at 2.5 dB

paths. The reliability of each path is described by a path metric. For q -ary polar codes, the path metric of \hat{u}^i is given by

$$\text{PM}(\hat{u}^i) = P_{U^i|\mathbf{Y}}(\hat{u}^i|\mathbf{y}) \quad (28)$$

and the recursive update rule is given by

$$\begin{aligned} \text{PM}(\hat{u}^i) &= P_{U^i|\mathbf{Y}}(\hat{u}^i|\mathbf{y}) \\ &= P_{U_i|\mathbf{Y}^{U^{i-1}}}(\hat{u}_i|\mathbf{y}^{\hat{u}^{i-1}}) P_{U^{i-1}|\mathbf{Y}}(\hat{u}^{i-1}|\mathbf{y}) \end{aligned} \quad (29)$$

$$= \underbrace{P_{U_i|\mathbf{Y}^{U^{i-1}}}(\hat{u}_i|\mathbf{y}^{\hat{u}^{i-1}})}_{\text{from (24)}} \text{PM}(\hat{u}^{i-1}) \quad (30)$$

where $\text{PM}(\hat{u}^0) = \text{PM}(\emptyset)$ is initialized to 1. Assuming L_{i-1} paths of length $i-1$ survive at the begin of decoding phase i . The SCL decoder first uses L_{i-1} parallel SC decoders to compute the PMF in (24) for all survived paths. Then $|\mathcal{S}(u_i)|L_{i-1}$ path metrics are computed by (30). The most likely L_i paths are selected as survivors and passed into phase $i+1$, where

$$L_i = \min(L, |\mathcal{S}(u_i)|L_{i-1}). \quad (31)$$

In our implementation, the “lazy copy” strategy is deployed to reduce copy operations and the path metrics are normalized as same as [4, Algorithm 10, lines 20-25] to avoid numerical problems.

The complexity of SCL decoding is dominated by the maximum list size L . In this work, we use the number of visited nodes in the decoding tree (N_{node}) and the number of path copies (N_{copy}) to evaluate the SCL decoding complexity. For conventional SCL decoding, we have

$$N_{\text{node}} = \sum_{i=1}^{n_c} L_i. \quad (32)$$

We observe that N_{node} is independent on the channel quality, which means the conventional SCL decoder does not adapt its complexity for different SNRs. An adaptive SCL decoder is proposed in [19]. The decoder is restarted by increasing the list size by a factor of 2 until the outputs contain at least one valid codeword.

We propose another approach to adapt the complexity by pruning the decoding tree in conventional SCL algorithm. The basic idea is to delete “unreliable” decoding paths although they are the L_i most likely. Let $\text{SPM}_i[l]$, $l = 1, \dots, L_i$ denote the sorted L_i largest path metrics ($\text{SPM}_i[1]$ is the largest). The path indexed by l is eliminated if at least one of the following conditions is fulfilled:

1. $\text{SPM}_i[l] < \delta_1 \text{SPM}_i[1]$
2. $\text{SPM}_i[l] < \delta_2 \text{SPM}_i[l-1]$

where

$$0 \leq \delta_1 \leq \delta_2 \leq 1. \quad (33)$$

The predefined parameters δ_1 and δ_2 describe a reliability requirement. If $\delta_1 = \delta_2 = 0$, this approach is equivalent to the conventional SCL decoder. If $\delta_1 = \delta_2 = 1$, this approach is equivalent to the SC decoder.

The performance and decoding complexity of SCL are shown in Fig. 8 (without CRC) and Fig. 9 (with CRC). We observe that the proposed SCL with a pruned decoding tree performs very close to the conventional SCL with significantly lower complexity. In the high SNR regime (≥ 2.25 dB), the average complexity converges to SC, i.e., $N_{\text{node, avg}} \approx N_{\text{node, SC}} = n_c$ and $N_{\text{copy, avg}} \approx N_{\text{copy, SC}} = 0$.

We also provide simulation results for binary polar codes in 5G [3] with same code length $n_{c, \text{bin}}$, dimension k and outer codes. Fig. 8 shows that q -ary polar codes provide better SC performance and distance properties than binary polar codes. In Fig. 9, we observe that q -ary polar codes can achieve the performance of binary polar codes with the list size reduced by a factor of 4.

IV. CONCLUSION AND FUTURE WORK

We discussed non-binary polar codes based on q -ary 2×2 kernels. The kernel is selected by maximizing the “single-level” polarization effect. The performance and complexity of BP, SCF and SCL decoding algorithms based on q -ary message passing are analyzed on biAWGN channels ($w = 1$).

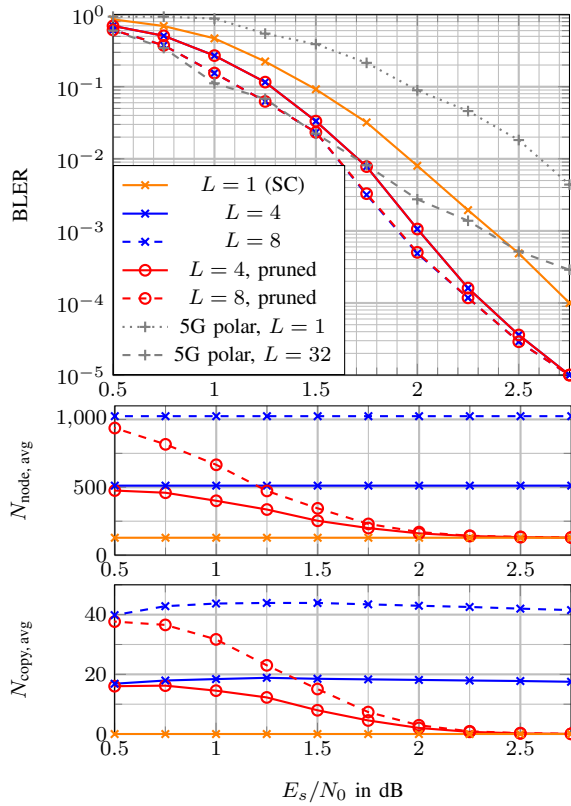


Figure 8: SCL decoding and SCL with a pruned tree for polar codes over GF(256) on a biAWGN channel ($w = 1$), $n_c = 128$, $k = 512$, no CRC, primitive polynomial = 285, $\alpha = 29$, $\beta = 1$, $\delta_1 = 10^{-6}$, $\delta_2 = 10^{-5}$, frozen position designed by Monte-Carlo method for SC decoding at 2.5 dB

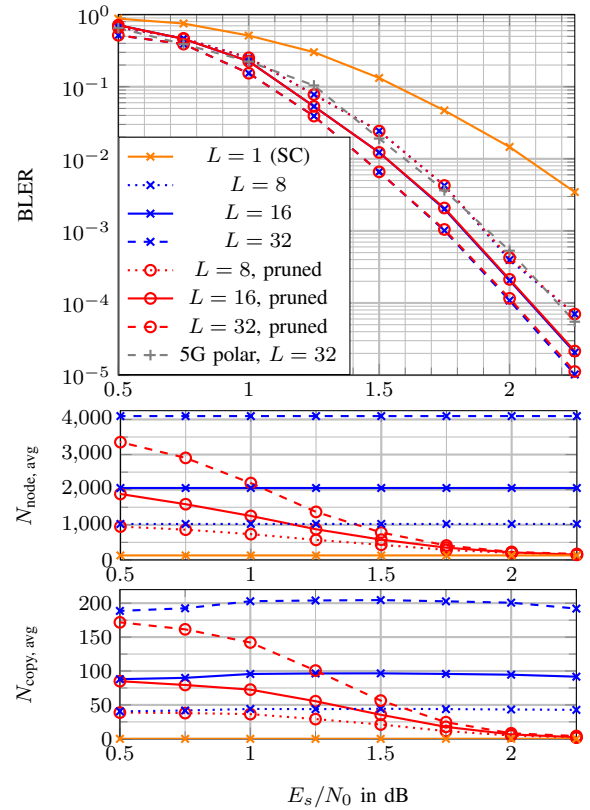


Figure 9: SCL decoding and SCL with a pruned tree for polar codes over GF(256) on a biAWGN channel ($w = 1$), $n_c = 128$, $k = 512$, $\ell_{\text{CRC}} = 16$, primitive polynomial = 285, $\alpha = 29$, $\beta = 1$, $\beta = 1$, $\delta_1 = 10^{-6}$, $\delta_2 = 10^{-5}$, frozen position designed by Monte-Carlo method for SC decoding at 2.5 dB

We proposed an SCL decoder with a pruned tree to adapt the decoding complexity.

The non-Monte-Carlo based code design (selection of frozen positions) and the analysis of non-binary polar codes for higher-order transmission ($1 < w \leq r$) will be investigated in the future.

REFERENCES

- [1] E. Arkan, "Channel polarization: A method for constructing capacity-achieving codes for symmetric binary-input memoryless channels," *IEEE Trans. Inf. Theory*, vol. 55, no. 7, pp. 3051–3073, Jul. 2009.
- [2] N. Stolte, "Rekursive Codes mit der Plotkin-Konstruktion und ihre Decodierung," Ph.D. dissertation, TU Darmstadt, 2002.
- [3] 3GPP TS 38.212, "3rd Generation Partnership Project (3GPP); Technical Specification Group Radio Access Network; New Radio; Multiplexing and channel coding (release 15)," Tech. Rep., Dec. 2017.
- [4] I. Tal and A. Vardy, "List decoding of polar codes," *IEEE Trans. Inf. Theory*, vol. 61, no. 5, pp. 2213–2226, May 2015.
- [5] O. Afisiadis, A. Balatsoukas-Stimming, and A. Burg, "A low-complexity improved successive cancellation decoder for polar codes," *48th Conf. on Signals, Systems and Computers*, pp. 2116–2120, Nov. 2014.
- [6] G. D. Forney, "Codes on graphs: Normal realizations," *IEEE Trans. Inf. Theory*, vol. 47, no. 2, pp. 520–548, Feb. 2001.
- [7] E. Arkan, "Polar codes: A pipelined implementation," in *Proc. 4th Int. Symp. on Broad. Commun. ISBC 2010*, 2010, pp. 11–14.
- [8] M. C. Davey and D. MacKay, "Low density parity check codes over GF(q)," *IEEE Commun. Lett.*, vol. 2, no. 6, pp. 165–167, Jun. 1998.
- [9] E. Şaşıoğlu, E. Telatar, and E. Arkan, "Polarization for arbitrary discrete memoryless channels," *IEEE Inf. Theory Workshop (ITW)*, pp. 144–148, Oct. 2009.
- [10] R. Mori and T. Tanaka, "Non-binary polar codes using reed-solomon codes and algebraic geometry codes," *IEEE Inf. Theory Workshop (ITW)*, pp. 1–5, Sep. 2010.
- [11] M.-C. Chiu, "Non-binary polar codes with channel symbol permutations," *Int. Symp. Inf. Theory and its Applicat. (ISITA)*, pp. 433–437, Oct. 2014.
- [12] P. Trifonov and V. Miloslavskaya, "Polar subcodes," *IEEE J. Sel. Areas Commun.*, vol. 34, no. 2, pp. 254–266, Feb. 2016.
- [13] L. Barnault and D. Declercq, "Fast decoding algorithm for LDPC over GF(2^q)," *IEEE Inf. Theory Workshop (ITW)*, pp. 70–73, Apr. 2003.
- [14] S. Cammerer, B. Leible, M. Stahl, J. Hoydis, and S. ten Brink, "Combining belief propagation and successive cancellation list decoding of polar codes on a GPU platform," *IEEE Inter. Conf. on Acoustics, Speech, and Sig. Process. (ICASSP)*, pp. 3664–3668, Mar. 2017.
- [15] B. Yuan and K. K. Parhi, "Early stopping criteria for energy-efficient low-latency belief-propagation polar code decoders," *IEEE Trans. on Signal Process.*, vol. 62, no. 24, pp. 6496–6506, Oct. 2014.
- [16] C. Poulliat, M. Fossorier, and D. Declercq, "Design of regular (2, d_c)-LDPC codes over GF(q) using their binary images," *IEEE Trans. Commun.*, vol. 56, no. 10, pp. 1626–1635, Oct. 2008.
- [17] N. Doan, S. A. Hashemi, M. Mondelli, and W. J. Gross, "On the Decoding of Polar Codes on Permuted Factor Graphs," *ArXiv e-prints*, Jun. 2018.
- [18] A. Elkelesh, M. Ebada, S. Cammerer, and S. ten Brink, "Belief Propagation List Decoding of Polar Codes," *ArXiv e-prints*, Jun. 2018.
- [19] B. Li, H. Shen, and D. Tse, "An adaptive successive cancellation list decoder for polar codes with cyclic redundancy check," *IEEE Commun. Lett.*, vol. 16, no. 12, pp. 2044–2047, Nov. 2012.